International Journal of Pharmaceutics 415 (2011) 273–283

Contents lists available at ScienceDirect

International Journal of Pharmaceutics

journal homepage: www.elsevier.com/locate/ijpharm

Pharmaceutical Nanotechnology

Lactoferrin conjugated PEG-PLGA nanoparticles for brain delivery: Preparation, characterization and efficacy in Parkinson's disease

Kaili Hu[a,b], Yanbin Shi[c], Wenming Jiang[d], Jiaying Han[a], Shixian Huang[a], Xinguo Jiang[a,*]

[a] Department of Pharmaceutics, School of Pharmacy, Fudan University, Shanghai 201203, People's Republic of China
[b] Murad Research Center for Modernized Chinese Medicine, Shanghai University of Traditional Chinese Medicine, Shanghai 201203, People's Republic of China
[c] School of Pharmacy, Lanzhou University, Lanzhou 730000, People's Republic of China
[d] Chemical Division, Shanghai Institute for Food and Drug Control, Shanghai 201203, People's Republic of China

ARTICLE INFO

Article history:
Received 6 January 2011
Received in revised form 4 May 2011
Accepted 24 May 2011
Available online 30 May 2011

Keywords:
Lactoferrin
Blood–brain barrier (BBB)
PLGA nanoparticles
Urocortin
Parkinson's disease

ABSTRACT

A novel biodegradable brain drug delivery system, the lactoferrin (Lf) conjugated polyethylene glycol-polylactide-polyglycolide (PEG-PLGA) nanoparticle (Lf-NP) was constructed in this paper with its *in vitro* and *in vivo* delivery properties evaluated by a fluorescent probe coumarin-6. Lf was thiolated and conjugated to the distal maleimide function surrounding on the pegylated nanoparticle to form Lf-NP. TEM observation and ELISA analysis confirmed the existence of active Lf on the surface of Lf-NP. The results of qualitative and quantitative uptake studies of coumarin-6 incorporated Lf-NP showed a more pronounced accumulation of Lf-NP in bEnd.3 cells than that of unconjugated nanoparticle (NP). Further uptake inhibition study indicated that the increased uptake of Lf-NP was via an additional clathrin mediated endocytosis processes. Following intravenous administration, a near 3 fold of coumarin-6 was found in the mice brain carried by Lf-NP compared to that carried by NP. Intravenous injection of urocortin loaded Lf-NP effectively attenuated the striatum lesion caused by 6-hydroxydopamine in rats as indicated by the behavioral test, the immunohistochemistry test and striatal transmitter content detection results. The cell viability test and CD68 immunohistochemistry demonstrated the acceptable toxicity of the system. All these results demonstrated that Lf-NP was a promising brain drug delivery system with reasonable toxicity.

1. Introduction

Drug delivery to the brain is made difficult by the presence of the blood–brain barrier (BBB) (Mehdipour and Hamidi, 2009; Pardridge, 2007). The endothelial cells of BBB form extremely tight junctions, providing a superfine filter that prevents the transport of most drugs from the vasculature into the brain parenchyma (De Boer and Gaillard, 2007). To overcome this, receptor-mediated drug delivery systems are developed by coupling of vectors with specific receptors on the BBB to drug loading vehicles. These systems combine the advantages of brain targeting, high incorporation capacity, reduction of side effects, and circumvention of the multidrug efflux system (Calvo et al., 2001; Jones and Shusta, 2007). The most well-known system, OX-26 conjugated immunoliposome, manifests extraordinary capacity of the receptor-mediated route by successful delivery of small molecular chemicals (Huwyler et al., 1996) and genes (Zhang et al., 2002, 2003) to the brain. However, the low stability of the liposome and disparity of the targeting effect of the monoclonal antibodies greatly impact its further application (Gosk et al., 2004; Moos and Morgan, 2001; Sharma and Sharma, 1997). Therefore, novel delivery systems are required to further increase brain delivery.

Lactoferrin (Lf) is a mammalian cationic iron-binding glycoprotein belonging to the transferrin (Tf) family. It exerts a number of biological functions such as anti-inflammatory, immunomodulatory and antimicrobial (Suzuki et al., 2005). Lf receptor (LfR) is found on the BBB of different species and transports Lf across the BBB *in vitro* and *in vivo* (Fillebeen et al., 1999; Huang et al., 2007; Suzuki et al., 2005). There are two classes of binding sites for Lf on cell membrane, a high affinity 105 kDa receptor protein and the low affinity glycosaminoglycans binding sites (Spik et al., 1994). Recently, Ji et al. (2006) demonstrated that the brain uptake of Lf was much higher than Tf and OX26. What is more, our previous studies using Lf as a brain targeting molecule resulted in successful brain delivery (Hu et al., 2009). These results proved Lf is a promising targeting molecule for improving brain delivery.

Urocortin (UCN), a corticotrophin releasing hormone related peptide, has recently been proposed as a cytoprotectant for cultured hippocampal neurons, cerebellar granule cells and GABAergic neurones (Choi et al., 2006; Facci et al., 2003; Pederson et al., 2002).

* Corresponding author. Tel.: +86 21 5198 0067; fax: +86 21 5198 0069.
E-mail address: xgjiang@shmu.edu.cn (X. Jiang).

0378-5173/$ – see front matter © 2011 Elsevier B.V. All rights reserved.
doi:10.1016/j.ijpharm.2011.05.062

Intravenous injected UCN could not across the BBB, while intracerebral injection of 20 fmol UCN was reported to be able to arrest the development of Parkinsonian like features in the rat 6-OHDA and lipopolysaccharide paradigms of Parkinson's disease, which indicating substantial therapeutic utility of UCN (Abuirmeileh et al., 2007; Kastin et al., 2000).

In this paper, Lf was conjugated to PEG-PLGA nanoparticles (NP) to construct a novel brain drug delivery system (Lf-NP). PEG-PLGA nanoparticles were chosen as the drug loading vehicles because of their better biodegradability over PEG-PLA nanoparticles. Coumarin-6 was incorporated into Lf-NP as a fluorescence probe to evaluate its brain targeting ability. The *in vitro* cell uptake, *in vivo* biodistribution and brain targeting behavior of Lf-NP were observed using HPLC fluorescence detection by tracking coumarin-6-loaded Lf-NP. Then, UCN was incorporated into Lf-NP to observe its therapeutic effect on Parkinson's disease. The toxicity of the system was also evaluated preliminarily by cell viability detection *in vitro* and by the CD68 immunohistochemisty *in vivo*.

2. Materials and methods

2.1. Materials and animals

Methoxy-poly (ethylene glycol) (MePEG, MW 3000 Da) was purchased from NOF Corporation (Japan) and Maleimide-PEG (MW 3500 Da) was custom-synthesized from Jenkem Technology (China). D,L-Lactide (purity: 99.5%) was purchased from PURAC (Netherlands). Glycolide was from Chengdu Organic Chemicals Co., Chinese Academy of Sciences (China). Sodium cholate was from Shanghai Chemical Reagent Company (China); Lactoferrin from Bovine Colostrum, 2-iminothiolane hydrochloride (2-IT), coumarin-6, rabbit anti-goat immunoglobulin (IgG) gold (10 nm) conjugate, urocortin, 6-hydroxydopamine (6-OHDA), dopamine hydrochloride, dihydroxyphenylacetic acid, homovanillic acid and dihydroxybenzylamine were all from Sigma–Aldrich (Saint Louis, MO, USA); VECTASTAIN® ABC Kit and DAB Substrate Kit for Peroxidase were from Vector Laboratories (Burlingame, CA, USA); Anti-tyrosine hydroxylase from Chemicon (Temecula, CA, USA); Urocortin (Rat) EIA Kit from Phoenix Pharmaceuticals (Mountain View, CA, USA); Rabbit anti-CD 68 antibody from Bioss Biotechnology (China); Goat anti-Bovine Lactoferrin-affinity purified and Bovine Lactoferrin Elisa Quantitation Kit were from Bethyl (Montgomery, TX, USA); 5,5-dithiobis (2-nitrobenzoic acid) (Ellman's reagent) from Acros (Belgium). Dulbecco's Modified Eagle Medium (high glucose) cell culture medium and plastic cell culture dishes, plates and flasks, from Corning Incorporation (Lowell, MA, USA); Fetal bovine serum (FBS) from Gibco (Carlsbad, CA, USA); Cell counting kit-8 (CCK-8) from Dojindo Laboratories (Japan); Tissue Tek® O.C.T. compound from Sakura Finetek USA Inc. (Netherlands). Double-distilled water was purified using a Millipore Simplicity System (Millipore, Bedford, MA, USA). All the other chemicals were of analytical reagent grades and used without further purification.

KM mice (18–20 g, ♂) were obtained from Experimental Animal Center of Fudan University. SD rats (200–250 g, ♂) and BALB/c mice (18–20 g, ♂) were from Sino-British SIPPR/BK Lab Animal Ltd. The animals were maintained at 22 ± 2 °C on a 12 h light-dark cycle with free access to food and water and were treated according to the protocols evaluated and approved by the ethical committee of Fudan University.

2.2. Preparation and characterization of NP and Lf-NP

2.2.1. Preparation of NP

The MePEG-PLGA and maleimide-PEG-PLGA copolymers were synthesized and characterized as described previously (Beletsi et al., 1999; Konstantinos, 2004). The double emulsion and solvent evaporation method was used to prepare the nanoparticles (NPs) (Lu et al., 2005). In brief, a primary emulsion was formed by emulsifying water in a dichloromethane solution of 0.0025 g maleimide-PEG-PLGA and 0.0225 g MePEG-PLGA on ice using a probe sonicator (Scientz Biotechnology Co. Ltd., China). Then the primary emulsion was subjected to intermissive sonication in 2 ml of a 1% sodium cholate aqueous solution on ice to form the w/o/w emulsion, which was further diluted into a 0.5% sodium cholate aqueous solution under magnetic stirring. The dichloromethane in the multiple emulsions was evaporated at low pressure and at 30 °C using Büchi rotavapor R-200 (Büchi, Germany). The formed nanoparticles were centrifuged at 21,000 × *g* for 45 min (TJ-25 centrifuge, Beckman Counter, USA) and the precipitation was resuspended in 0.5 ml of a 0.01 M HEPES buffer pH 7.0 containing 0.15 M NaCl for further use. The coumarin-6 and the UCN loaded nanoparticles were prepared with coumarin-6 (0.01% or 0.003%, w/v, to the dichloromethane solution) or UCN (0.4%, w/v, to the inner water phase) added before primary emulsification. In addition, the coumarin-6 loaded nanoparticles were subjected to a 1.5 cm × 20 cm sepharose CL-4B column and eluted with 0.05 M HEPES buffer pH 7.0 containing 0.15 M NaCl to remove the unentrapped coumarin-6. Other experimental conditions were the same as described above.

2.2.2. Preparation of Lf-NP

The Lf was thiolated and purified as described previously (Hu et al., 2009). The purified thiolated Lf was added to the NPs and incubated at room temperature for 9 h to prepare the Lf-NP. The solution was then subjected to a 1.5 cm × 20 cm sepharose CL-4B column and eluted with 0.01 M phosphate buffered saline (PBS) buffer pH 7.4 to remove the unconjugated thiolated Lf.

2.2.3. Morphology, particle size and zeta potential

The mean diameter and zeta potential of the nanoparticles were determined by a Zeta Potential/Particle Sizer NICOMP™ 380 ZLS (PSS.NICOMP PARTICLE SIZE SYSTEM, Santa Barbara, CA, USA). A transmission electron microscope (TEM, H-600, Hitachi, Japan) was used for the morphological examination of the nanoparticles.

2.2.4. TEM of gold-labeled Lf-NP

To demonstrate the existence of Lf on the surface of Lf-NP, Lf-NP was sequentially incubated with two antibodies: 20 μl 1 μg/ml goat anti-bovine Lf primary antibody and 50 μl 10 nm colloidal gold-labeled rabbit anti-goat secondary antibody. The NP and Lf-NP treated without the primary antibody were subjected to the same procedure and served as negative controls. Then they were stained with 1% (w/v) phosphotungstic acid solution and examined under TEM.

2.2.5. Conjugated Lf number and drug loading capacity

The average number of Lf molecules conjugated per nanoparticle was calculated by dividing the number of Lf molecules which were determined by a Lactoferrin ELISA Kit, by the average number of nanoparticles determined as described previously (Olivier et al., 2002). The nanoparticle concentration was determined by turbidimetry using UV2401 spectrophotometer at 350 nm (Shimadzu, Japan). The coumarin-6 loading capacity (CLC) of NP and Lf-NP were determined by HPLC analysis after dissolving them in a 20 times volume of methanol (Lu et al., 2005). While the UCN loading capacity (ULC) of NP and Lf-NP was calculated by detecting the UCN content in the supernatant after centrifugation by an Urocortin ELISA Kit.

2.2.6. Stability of the fluorescent probe

To evaluate if the fluorescence probe remained associated with the particles during a 24 h incubation period, the *in vitro* release of coumarin-6 from the nanoparticles was investigated under sink condition. Coumarin-6-loaded Lf-NP and NP were incubated at 37 °C in pH 4 and pH 7.4 PBS, which represented the pH in the endo-lysosomal compartment and physiologic pH respectively, at a coumarin-6 concentration of 50 ng/ml with a shaking rate at 100 rpm. Periodic samples were subject to centrifugation at 21,000 × *g* for 45 min and the supernatant was further diluted with methanol and analyzed for the released coumarin-6 by HPLC assay.

2.3. In vitro uptake of coumarin-6-loaded NP and Lf-NP by bEnd.3 cells

2.3.1. Cell culture

The immortalized mouse brain endothelial cell line b.End3 was cultured in 10 cm tissue culture dishes in Dulbecco's Modified Eagle Medium containing 10% FBS, penicillin (100 U/ml) and streptomycin (100 mg/ml).

2.3.2. Fluorescent microscopy of coumarin-6-loaded Lf-NP and NP uptake by bEnd.3 cells

bEnd.3 cells were seeded at a density of 10^4 cells/cm^2 on the polylysine-coated glass cover slip. On the second day, pre-incubated with HBSS for 15 min, the medium was replaced with coumarin-6-loaded Lf-NP and NP suspensions (10 μg/ml in HBSS, pH 7.4) following by incubation for 0.25, 0.5 and 1 h at 37 °C, respectively (Davda and Labhasetwar, 2002; Panyam et al., 2003). Then the cells were washed three times with PBS and fixed with 4% paraformaldehyde solution for 20 min. After washing three times with PBS, the cells were mounted in Dako fluorescent mounting medium and observed under fluorescent microscope (Olympus, Japan).

2.3.3. Quantitative analysis of the uptake of coumarin-6-loaded Lf-NP and NP by bEnd.3 cells

bEnd.3 cells were seeded at a density of 10^5 cells/cm^2 onto 24-well plates. On the second day, pre-incubated with HBSS for 15 min, the medium was replaced with the suspension of nanoparticles (1–60 μg/ml) and incubated for 1 h at 4 °C and 37 °C, respectively, to study the effect of incubation temperature on nanoparticle uptake. In a separate experiment, to study the effect of incubation time on nanoparticle uptake, the medium was replaced with 1 ml 10 μg/ml suspension of nanoparticles in HBSS per well and the plate was incubated for 15 min, 30 min, 1 h, 2 h and 4 h at 37 °C, respectively. For uptake inhibition experiment, 10 mg/ml Lf and different endocytic inhibitors (2.6 mg/ml NaN_3, 10 μg/ml filipin, 20 μg/ml chlorpromazine, 4 μg/ml colchicines, 20 μg/ml BFA and 140 ng/ml monensin) were added with 10 μg/ml Lf-NP suspension and incubated for 30 min at 37 °C, respectively. Then the cells were washed with ice-cold PBS for five times and solubilized in 400 μl 1% Triton X-100. Twenty-five microliters of the cell lysates from each well were subjected to BCA protein assay (Shanghai Shenergy Biocolor Bioscience and Technology Co., Ltd., China). One hundred microliters of the cell lysates were lyophilized and used for HPLC analysis of coumarin-6 after extraction by 1 ml methanol. A standard curve of nanoparticles was constructed by suspending different concentrations of nanoparticles (6–1200 ng/ml) in 1% Triton X-100 followed by lyophilization and extraction of coumarin-6 in methanol. The uptake of nanoparticles by bEnd.3 cells was calculated from the standard curve and expressed as the amount of nanoparticles (μg) uptaken per mg cell protein.

2.4. Biodistribution of coumarin-6-loaded NP and Lf-NP

2.4.1. Qualitative studies

Coumarin-6-loaded Lf-NP and NP were injected into the caudal veins (dose 60 mg/kg) of mice, respectively. After 1 h, the mice were anaesthetized and frozen brain sections of 20 μm thickness were prepared and stained with 1 μg/ml DAPI for 10 min at room temperature. After PBS washing, the sections were mounted in Dako fluorescent mounting medium and examined under the fluorescence microscope (Olympus, Japan).

2.4.2. Quantitative studies

Fifty-four mice were randomly divided into two groups, receiving coumarin-6 loaded Lf-NP and NP nanoparticles, respectively. The animals were injected in tail vein with a dose of 60 mg/kg fluorescence-loaded nanoparticles. At 0.083, 0.25, 0.5, 1, 2, 4, 8, 12 and 24 h following i.v. injection, the blood samples were collected and the mice were sacrificed. The brain, heart, liver, spleen, lung and kidney tissues were harvested following by quick washing with cold saline and then subjected to n-hexane extraction for HPLC analysis with coumarin-7 as the internal standard.

Concentration data were dose-normalized and plotted as probe concentration–time curves in the blood and different tissues. The C_{max}, T_{max} values were read directly from the concentration–time profile and the area under the concentration–time curve (AUC_{0-t}) was calculated by the trapezoidal rule. The statistical differences between Lf-NP and NP were assessed using an unpaired Student's *t* test and a *P* value of less than 0.05 was accepted as significant.

2.5. Therapeutic effect of urocortin-loaded Lf-NP on 6-OHDA rat model of Parkinson's disease

2.5.1. Unilateral intrastriatal infusion of 6-OHDA

For the stereotaxic surgery, rats were anaesthetized by chloral hydrate (400 mg/kg i.p.) and then positioned in a stereotaxic frame (Narishige, Japan) to achieve a flat skull position. A sagittal incision was made in the scalp with sterile blade, then the skin and inferior tissue layers covering the skull were retracted and a small hole was drilled at the following coordinates: lateral (L) 3 mm, antero-posterior (AP) 0.2 mm, from the bregma point. The stereotaxic co-ordinates were calculated for the striatal region following the "Rat Brain Atlas" (Paxinos and Watson, 1998). The 6-OHDA solution (10 μg/ml in 1% ascorbic acid) was infused unilaterally through a stainless steel cannula into the striatal region (dorso-ventral 4.8 and 5.6 mm from the bregma point) at 0.3 μl/min, 1.5 μl each point. Animals were allowed to recover completely before being returned to housing.

2.5.2. Experimental design

Ninety rats were randomly divided into nine groups. Eight groups were unilaterally infused with 6-OHDA to the striatum while the other group given no treatment was served as normal control. On the next day, different treatments were given to the rats as shown in Table 1. All rats were subjected to behavior test 7, 14 and 21 days after 6-OHDA infusion. After the last behavior test, the rats were sacrificed and the brains were harvested for immunohistochemistry stain of tyrosine hydroxylase and HPLC detection of the striatal neurotransmitters.

2.5.3. Rotational behavior

On the 7th, 14th and 21st day after intrastriatal injection of 6-OHDA, 0.5 mg/kg apomorphine was subcutaneously injected to the neck of rat in each groups and 5 min later, the completed 360° circle turns toward the intact side were counted continuously for 30 min. The whole experiment processes were under double blind conditions.

Table 1
Treatments given to different groups in the 6-OHDA PD model study.

Groups	Treatments
PBS	6-OHDA lesion, i.v. injection of 0.5 ml PBS
Lf-NP-UCN1	6-OHDA lesion, i.v. injection of 5.6 μg UCN carried by Lf-NP
Lf-NP-UCN3	6-OHDA lesion, i.v. injection of 16.8 μg UCN carried by Lf-NP
Lf-NP-UCN5	6-OHDA lesion, i.v. injection of 28 μg UCN carried by Lf-NP
NP-UCN5	6-OHDA lesion, i.v. injection of 28 μg UCN carried by NP
Blank NP	6-OHDA lesion, i.v. injection of blank NP
Blank Lf-NP	6-OHDA lesion, i.v. injection of blank Lf-NP
UCN	6-OHDA lesion, i.v. injection of 28 μg UCN solution
Normal	None

2.5.4. Tyrosine hydroxylase immunohistochemistry

After the behavioral test on the 21st day, two rats of each group were anaesthetized with chloral hydrate, and perfused intracardially with 0.1 M PBS pH 7.4 followed by 4% paraformaldehyde in PBS. Then brains were removed, kept in 4% paraformaldehyde fixative for 12 h, and cryoprotected in 30% sucrose PBS solutions for 24 h at 4 °C. Serial coronal sections (30 μm thickness) were made, free-floated in PBS, and processed for tyrosine hydroxylase immunohistochemistry as described below.

The sections were rinsed with 0.1 M PBS, pH 7.4, permeabilized in 0.25% Triton X-100 for 30 min, incubated in 0.3% H_2O_2 for 15 min, and blocked by incubating for 2 h in normal goat serum. After rinsing with PBS, sections were incubated with the primary antibody (anti-tyrosine hydroxylase, 1:200; Chemicon Inc., USA) in PBS overnight at 4 °C. The next day, after rinsing in PBS, sections were treated with the VECTASTAIN® ABC Kit (Vector Laboratories, USA). After development with 3,3′-diaminobenzidine solution (Vectastain DAB kit, Vector Laboratories, USA) for 8 min, all sections were washed for 10 min in double distilled water, mounted on slides, dried, dehydrated in graded ethanol, cleared in xylene, and mounted with resinene and observed under microscope (UFX-II, Nikon, Japan).

2.5.5. HPLC detection of striatal dopamine and its metabolites

After the behavior test on the 21st day, eight rats of each group were sacrificed with each left and right striata harvested separately for the assay of dopamine (DA) and its main metabolites dihydroxyphenylacetic acid (DOPAC) and homovanillic acid (HVA) as described previously (Huang et al., 2010). Briefly, each striatum was deproteinized following 20 s sonication in 0.2 M $HClO_4$ containing 0.2 mmol/l $Na_2S_2O_5$ and 0.01% EDTA-2Na (1 ml/100 mg tissue). The samples were centrifuged at 10,000 × *g* for 10 min, and the supernatants were passed through a 0.22 μm syringe filter before injecting into the HPLC system (Agilent 1100, Agilent Technologies, USA) equipped with a electrochemical detector (Coulochem III, ESA, USA). The composition of mobile phase was 40 mM sodium acetate, 15 mM citric acid, 0.25 mM sodium octanesulfonate, 0.2 mM EDTA-2Na, and 16% methanol (pH 4.3). The amount of DA, DOPAC and HVA were quantified using a standard curve with DHBA as internal standard and represented as ng/g wt. The percent contents of DA, DOPAC and HVA were calculated by dividing the content in the lesioned striatum by that in the unlesioned side, respectively.

2.6. Preliminarily evaluation of the in vitro and in vivo toxicity of Lf-NP

To evaluate the cytotoxicity of Lf-NP preliminarily *in vitro*, cell viability of bEnd.3 cells after contacting with different concentra-

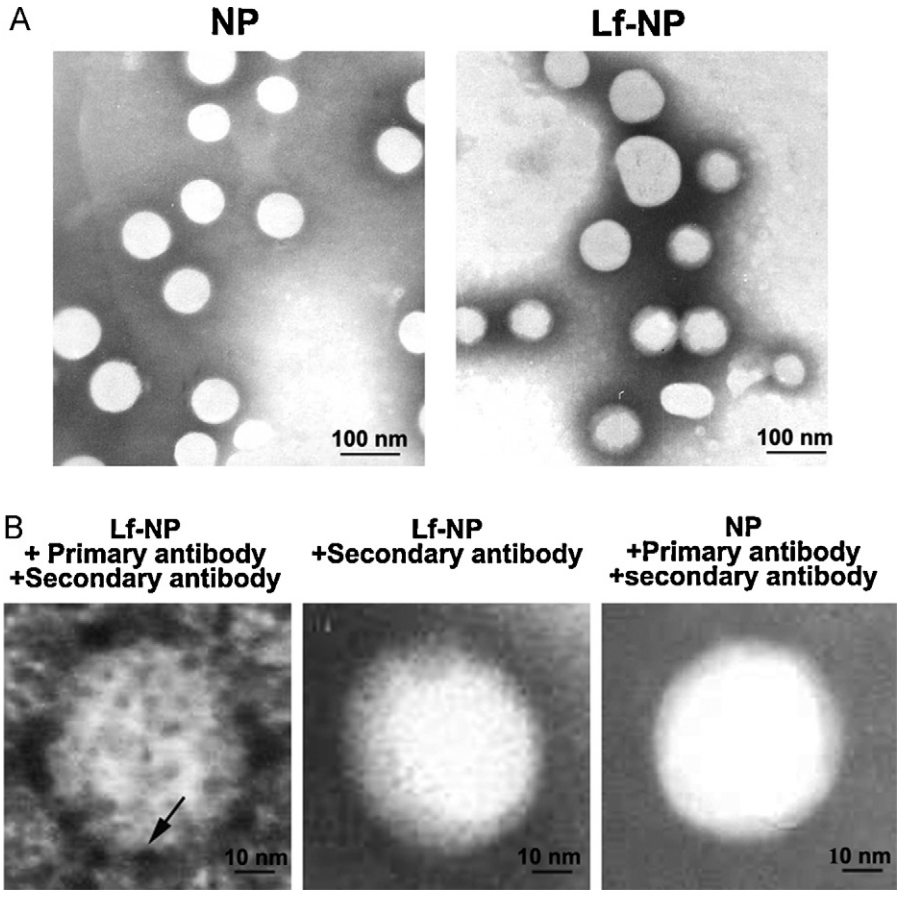

Fig. 1. Transmission electron micrograph of different nanoparticles negatively stained with phosphotungstic acid solution. (A) NP and Lf-NP. (B) Lf-NP and NP after incubated with different antibodies.

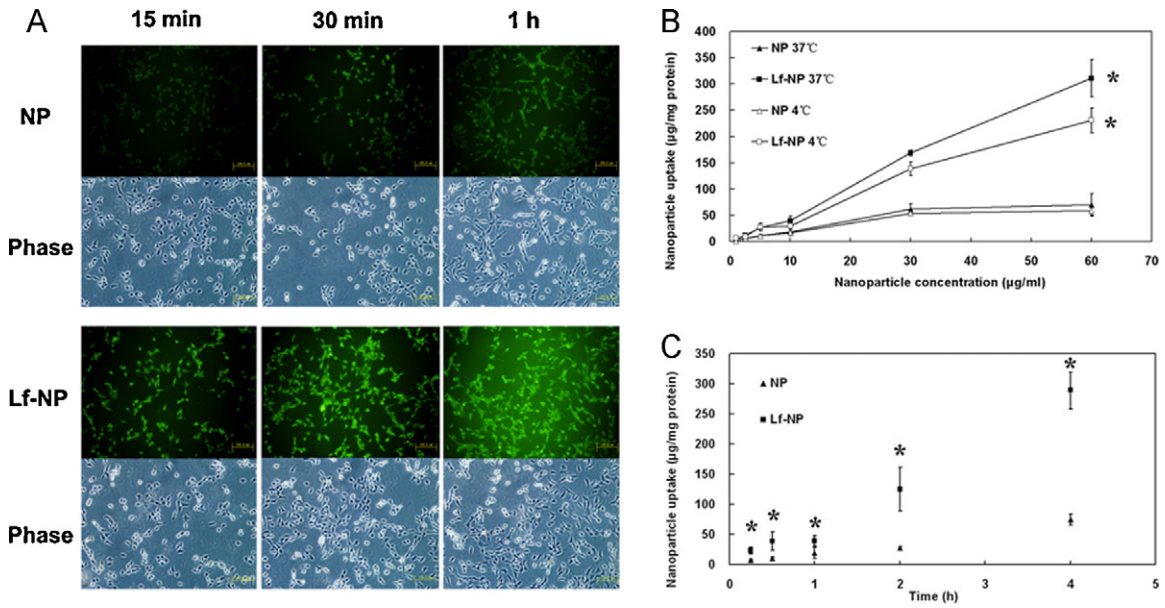

Fig. 2. *In vitro* bEnd.3 uptake results of coumarin-6 loaded Lf-NP and NP. (A) 10 μg/ml at 37 °C for different times. Below each fluorescent photo is their corresponding phase contrast photo. The magnification bar is 100 μm. (B) 1–60 μg/ml incubation for 1 h at 37 °C and 4 °C. (C) 10 μg/ml at 37 °C for different times. Results shown are mean ± SD ($n = 3$) $^*p < 0.05$.

tions of Lf-NP was evaluated by MTT hydrolysis using CCK-8. Lf, NP and Lf-NP of 0.025 to 3.0 mg/ml in PBS (pH 7.4) were incubated with the cells for 4 h at 37 °C and cell viability was expressed as percentage of absorbance at 450 nm in comparison with that of the control, which comprised the cells without exposure to the samples.

The acute inflammation caused by Lf-NP *in vivo* was evaluated by CD68 immunochemistry. The BALB/c mice were injected with unloaded Lf-NP at the dose of 180 mg/kg/day and 60 mg/kg/day for 7 successive days, respectively. Twenty-four and forty-eight hours post last dose, the animals were anaesthetized and perfused intracardially with 0.9% NaCl followed by 4% paraformaldehyde. Cerebrum, cerebellum, heart, liver, spleen, lung and kidney were removed to prepare paraffin-embedded sections (5 μm thickness) according to standard laboratory techniques. Following deparaffinized through xylenes and ethanol, sections were treated with microwave heating in 0.01 M citrate buffer (pH 6.0) at 95 °C for double 5 min in a microwave oven (Glanz WD900ESL23I-3, Guangdong, China) with a power setting of 780 W to retrieve antigens. Immunohistochemistry was performed using 1:200 dilution of rabbit anti-mouse CD 68 antibody overnight at 4 °C followed by the VECTASTAIN® ABC Kit. The slides were observed under a microscope after developed with DAB and counter-stained with hematoxylin.

3. Results and discussion

3.1. Preparation and characterization of NP and Lf-NP

The average molecular weight of the synthesized maleimide-PEG_{3500}-PLGA and $MePEG_{3000}$-PLGA detected by ^1H NMR spectroscopy were 35,906 and 32,851, respectively, with a PGA to PLA ratio of 50:50. The particle size of NP and Lf-NP were both about 90 nm with the zeta potentials of around −24 mV. After coumarin-6 and UCN encapsulation, the nanoparticle size raise to around 95 nm and 120 nm, respectively. Generally, the size of brain delivery nanoparticles is controlled under 200 nm to facilitate the endocytosis by the brain capillary cells (Calvo et al., 2001; Olivier et al., 2002). The size of the prepared NP and Lf-NP was all below 150 nm that was regarded as favorable to brain transport. The zeta potential of UCN encapsulated nanoparticles changed to about −14 mV, which was in accordance with published results of protein encapsulated PEG-PLGA nanoparticles (Li et al., 2001). The UCN-loaded nanoparticles had a relatively positive zeta potential compared with the unloaded ones, which might cause some disparity in their behavior *in vitro* and *in vivo*. However, both neutral and negatively charged surface nanoparticles have reduced plasma protein adsorption and low rate of nonspecific cellular uptake (Alexis et al., 2008). As the zeta potentials of the loaded and unloaded nanoparticles were both negative, we supposed there may not be significant difference between their *in vitro* and *in vivo* behavior.

TEM photographs showed the NP and Lf-NP were both spherical and of regular size (Fig. 1A). Gold particles were observed under TEM around the surface of Lf-NP incubated with an anti-Lf primary antibody and a 10 nm colloidal gold-labeled secondary antibody sequentially (Fig. 1B), which proved the preservation of receptor binding ability of the conjugated Lf. The active Lf on the nanoparticle surface would ensure the targeting effects of Lf-NP to the Lf receptor on brain capillaries. The specificity of this immunostaining procedure was validated by negative controls with no gold particle on the nanoparticle surface (Fig. 1B). The average Lf number on each Lf-NP determined by a Lactoferrin ELISA Kit was around 42.

When 0.003% or 0.01% (w/v) of coumarin-6 was added, the CLC was 0.072% and 0.79% for NP, 0.066% and 0.56% for Lf-NP, respectively. The nanoparticles with lower CLC were used in cell uptake experiments while those with higher CLC were used in *in vivo* experiments. The ULC of UCN-loaded NP and Lf-NP detected by the UCN ELISA Kit was 0.33% and 0.28%, respectively.

The results of the *in vitro* release study conducted in pH 4.0 and pH 7.4 PBS at 37 °C showed that no more than 4% of coumarin-6 was released from NP and Lf-NP after a 24 h incubation period, which was in consistent with previous studies (Hu et al., 2009; Lu et al., 2005). These results suggested the stability of the incorporated coumarin-6 in the nanoparticles and indicated that the fluorescence signal detected in the cell or tissue samples was mainly attributed to the coumarin-6 encapsulated into the nanoparticles.

3.2. In vitro uptake of coumarin-6-loaded NP and Lf-NP by bEnd.3 cells

Unlike primary cultures cells that are grow slowly, prone to contamination by other neurovascular unit cells, and lose blood–brain

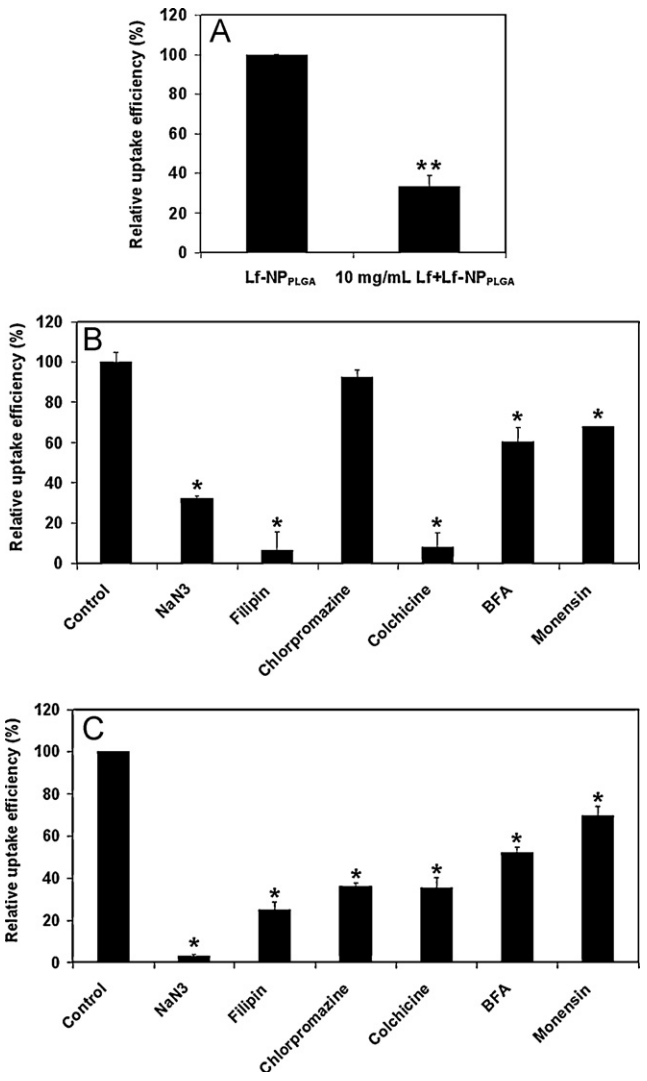

Fig. 3. Relative uptake efficiency of NP and Lf-NP by bEnd.3 cells after incubated with different uptake inhibitors for 30 min at 37 °C. (A) 10 mg/ml Lf; (B) NP after incubation with different inhibitors. (C) Lf-NP after incubation with different inhibitors. Data are mean ± SD, $n = 3$, $^*p < 0.05$ corresponding to the control group.

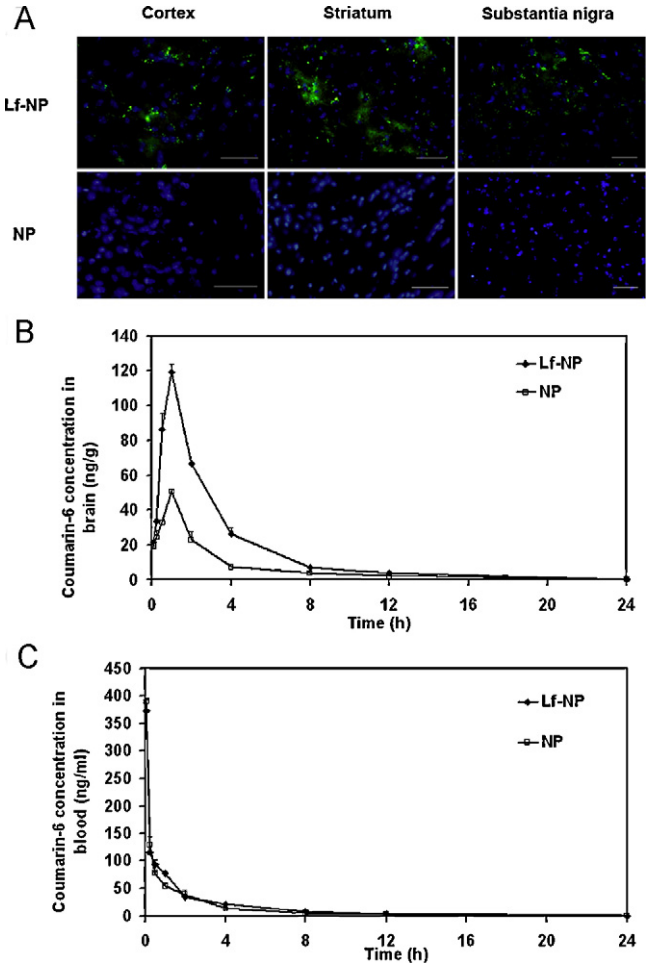

Fig. 4. *In vivo* brain uptake results of 60 mg/kg coumarin-6 loaded NP and Lf-NP. (A) The green fluorescence signals of coumarin-6 were visualized using the FITC filter of brain sections 1 h after nanoparticle injection. The blue cell nuclei were stained with 1 μg/ml DAPI for 10 min and visualized using the UV filter. The bar on each photo is 50 μm. (B) Concentrations–time curve of coumarin-6 in cerebrum followed by i.v. NP or Lf-NP in mice. (C) Concentrations–time curve of coumarin-6 in whole blood followed by i.v. NP or Lf-NP in mice. In both (B) and (C), data represented the mean ± SD, $n = 3$.

barrier characteristics when passaged, bEnd.3 cells are an attractive candidate as a model of the BBB due to their rapid growth, maintenance of blood–brain barrier characteristics over repeated passages, formation of functional barriers and amenability to numerous molecular interventions (Brown et al., 2007). Here it was chosen as an easy BBB model to study the brain delivery property of Lf-NP *in vitro*. The endothelial properties of bEnd.3 were confirmed by immunochemistry stain of factor VIII and ZO-1, and the TEER of the cell layer was confirmed to be around 100 Ω cm^2 (similar to the reported value) in preliminary studies. All comparisons of NP and Lf-NP uptake were carried out by using the same culture.

The *in vitro* uptake results showed that the uptake of Lf-NP by bEnd.3 cells was time-, temperature- and concentration-dependant which suggested an endocytosis process. The uptake of Lf-NP by bEnd.3 cells was higher than the uptake of NP during the 4 h incubation period, about 3.9 times higher than that of NP at 4 h (Fig. 2C). The uptake amount of Lf-NP under 37 °C was much higher than that under 4 °C. At both 4 °C and 37 °C, the uptake of Lf-NP increased with increase in the concentration, showing almost a first order kinetics. At 60 μg/ml concentration, the uptake amount of Lf-NP reached 4.43 and 3.94 times of those of NP at 4 °C and 37 °C, respectively (Fig. 2B).

The enhanced uptake of Lf-NP than NP by bEnd.3 cells could be explained by an additional endocytosis mechanism involving Lf. To confirm this, excess free Lf (10 mg/ml) was added with Lf-NP and incubated at 37 °C for 30 min. The relative uptake efficiency, which was calculated by dividing the uptake amount of nanoparticle with inhibitors by that without inhibitors, was used to evaluate the inhibitory effect of the Lf on Lf-NP uptake. The relative uptake effi-

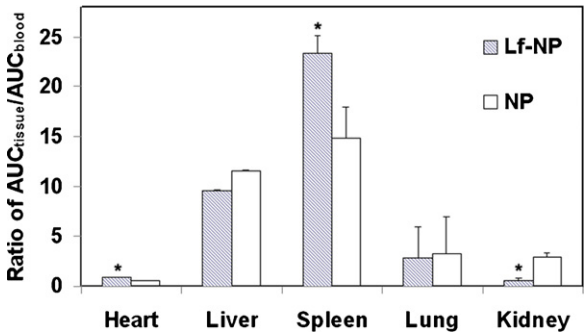

Fig. 5. Tissue distribution of Lf-NP and NP denoted as AUC$_{tissue}$/AUC$_{blood}$. Data are mean ± SD, $^*p < 0.05$ corresponding to the NP.

Table 2
Pharmacokinetic parameters of coumarin-6 in brain and whole blood following i.v. injection of coumarin-6 loaded NP or Lf-NP in mice.

PK parameters	Blood		Brain	
	NP	Lf-NP	NP	Lf-NP
k (h^{-1})[a]	0.38 ± 0.15	0.54 ± 0.08	0.38 ± 0.11	0.52 ± 0.07
$t_{1/2}$ (h)[a]	1.83 ± 0.72	1.27 ± 0.19	1.85 ± 0.53	1.35 ± 0.18
T_{max} (h)	0	0	1	1
C_{max} (ng/g or ng/ml)	388.24 ± 7.25	372.50 ± 22.55	50.57 ± 0.69	119.54 ± 4.67[b]
$AUC_{(0-t)}$ (ng/(g h) or g/(ml h))	290.17 ± 27.81	329.81 ± 28.37	149.73 ± 8.91	372.13 ± 15.71[b]

[a] k and $t_{1/2}$ denotes elimination rate constant and elimination half life respectively.
[b] Mean ± SD Significantly different from NP, $p < 0.05$.

ciency of Lf-NP with Lf was merely 30% of Lf-NP, which proved the significant effect of Lf on Lf-NP uptake (Fig. 3A). For further elucidating the uptake mechanism of Lf-NP, different endocytic inhibitors were added with Lf-NP and NP and their effects on nanoparticle uptake were evaluated by the relative uptake efficiency. There were three major pathways for nanoparticles under 200 nm to be endocytosed by cells, which is by the clathrin or the caveolae on the cell membrane and by macropinocytosis (Seto et al., 2002). Chlorpromazine, which prevented the assembly of coated pits at the cell membrane and filipin, a sterol-binding agent that disrupted caveolar structure and function were used to inhibit clathrin-dependent and caveolae-dependent processes, respectively (Mo and Lim, 2004). NaN_3 which could exhaust ATP was used to cause energy depletion (Legen et al., 2003). Colchicine which played a role for microtubules and microfilaments was a typical inhibitor of the macropinocytosis pathway (Liu and Shapiro, 2003). While BFA which could destruct the structure and function of Golgi apparatus and monensin, a inhibitor to the acid environment of lysosome were used to judge if the endocytosis process was related to Golgi apparatus and lysosome, respectively (Gabor et al., 2002; Grau et al., 2001). The uptake inhibition experiment results are shown in Fig. 3. Both the uptake of NP and Lf-NP were inhibited by NaN_3, filipin, colchicines, BFA and monensin, which suggested their endocytosis was a Golgi apparatus, lysosome, caveolae and macropinocytosis related process. Unlike NP, the uptake of Lf-NP was also inhibited by chlorpromazine, which indicated the introduction of Lf endowing the system with an additional clathrin mediated endocytosis process.

The above findings demonstrated the Lf induced and clathrin mediated endocytosis mechanism for enhanced uptake of Lf-NP. Lf receptor had been proved extensively on brain capillary endothelial cells and brain membrane preparations (Fillebeen et al., 1999; Huang et al., 2007; Suzuki et al., 2005). There were also interesting reports showed that the expression of Lf receptor in the brain increased under some disease conditions such as Parkinson's disease and Alzheimer's disease, indicating Lf-NP could be developed for delivery of therapies to treat these diseases (Faucheux et al., 1995; Grau et al., 2001; Kawamata et al., 1993).

Fluorescent microscopy photographs of bEnd.3 cells exposed to Lf-NP and NP at the same concentration are shown in Fig. 2A. The increase of fluorescent intensity in the cells correlated with increase in the time of incubation. After incubation for 15, 30 and 60 min at 37 °C, respectively, there was a significantly accumulated amount of dye of Lf-NP in the cells compared with that of NP. In preliminary experiments, we observed the cell uptake of free coumarin-6 and the fluorescent signal of free coumarin-6 could be neglected compared with that of nanoparticles containing the same amount of coumarin-6. Previous studies also proved that free dye released from PLGA nanoparticles accounted for only about 3% of the total uptake of the dye after 2 h of incubation (Davda and Labhasetwar, 2002). In addition, our *in vitro* release results demonstrated the stability of the coumarin-6 in the nanoparticles. So we concluded that coumarin-6 detected in the cells dominantly reflected the nanoparticles.

3.3. Biodistribution of coumarin-6-loaded NP and Lf-NP

Microscopic observation of coronal sections of the mice brain showed that there was certain amount of Lf-NP incorporated coumarin-6 distributed in the cortex, substantia nigra and striatum region 1 h after injection, while the fluorescence of NP in these regions was almost undetectable (Fig. 4A). This proved that Lf conjugation endowed Lf-NP with the ability of reach the brain parenchyma through the endothelial cells of BBB. Based on our cell uptake results, this might be induced by an extra clathrin-related transport mechanism. Substantia nigra and striatum regions are the major pharmacological targets for Parkinson's disease, so Lf-NP could be adopted to deliver drug therapy for Parkinson's disease.

To evaluate the biodistribution of Lf-NP and NP, coumarin-6 was incorporated into the nanoparticles, and the blood and tissue concentrations of the fluorescent marker were detected with a validated HPLC-fluorescence detection method. The results showed that the brain uptake of coumarin-6 associated to both Lf-NP and NP exhibited similar concentration–time profiles (Fig. 4B), and the AUC and C_{max} of coumarin-6 in the brain by Lf-NP was about 2.49 and 2.36 folds compared with that by NP, respectively (Table 2). This

Table 3
Pharmacokinetic parameters of coumarin-6 in different tissues following i.v. NP and Lf-NP in mice, respectively (mean ± SD, $n = 3$, $p < 0.05$*).

Tissue	k (h^{-1})	$t_{1/2}$ (h)	C_{max} (ng/g)	T_{max} (h)	AUC_{0-t}
NP					
Heart	0.62 ± 0.16	1.11 ± 0.29	111.94 ± 0.40	0.08333	163.88 ± 13.77
Liver	0.79 ± 0.12	0.88 ± 0.14	3334.18 ± 324.86	0.08333	3351.55 ± 844.21
Spleen	1.48 ± 0.59	0.48 ± 0.19	4544.57 ± 529.90	0.25	4298.65 ± 975.77
Lung	0.35 ± 0.09	1.95 ± 0.51	322.12 ± 43.40	0.5	952.62 ± 99.67
Kidney	1.43 ± 0.15	0.48 ± 0.05	81.73 ± 17.09	1	851.05 ± 67.72
Lf-NP					
Heart	0.79 ± 0.41	0.87 ± 0.46	152.20 ± 0.01*	0.5	308.29 ± 10.04*
Liver	0.76 ± 0.11	0.91 ± 0.13	4655.53 ± 434.55*	0.08333	3167.365 ± 560.79
Spleen	1.39 ± 0.68	0.50 ± 0.25	5420.06 ± 387.43	0.25	7680.99 ± 769.38*
Lung	0.49 ± 0.09	1.41 ± 0.27	550.20 ± 6.59*	0.25	943.06 ± 29.01
Kidney	0.43 ± 0.21*	1.63 ± 0.84	378.95 ± 36.52*	0.5	181.71 ± 26.64*

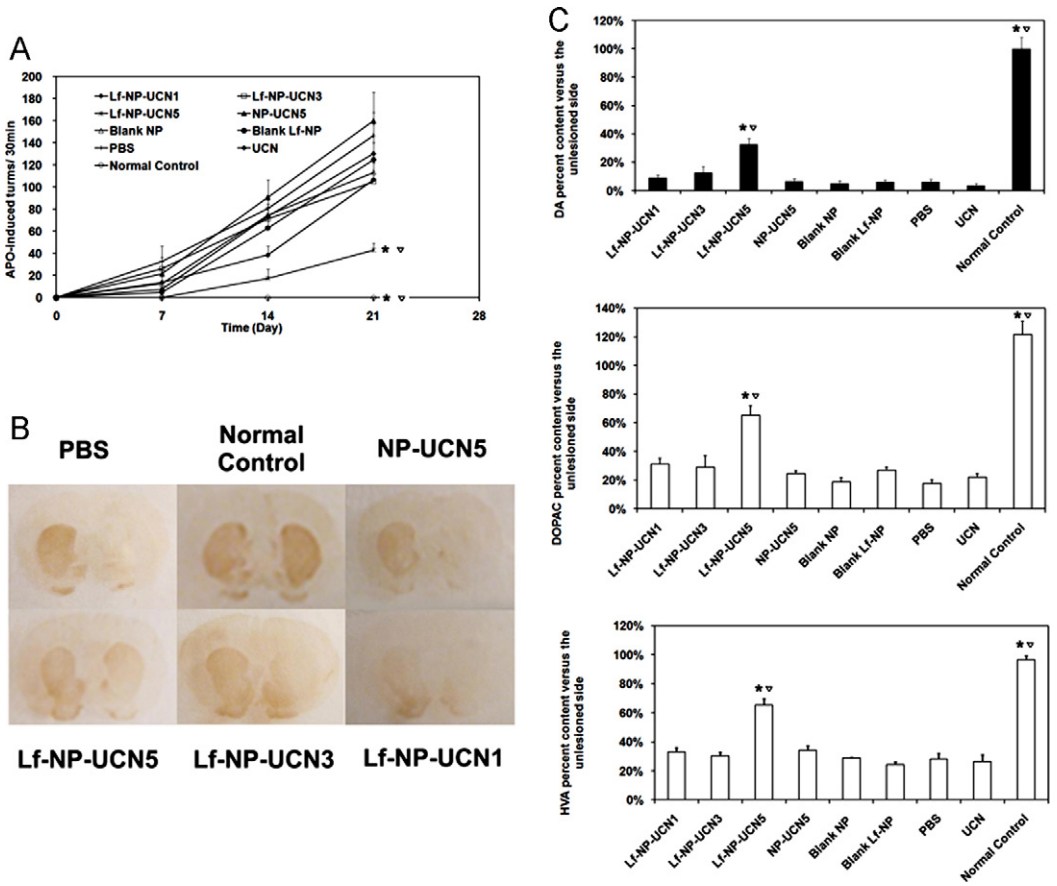

Fig. 6. Therapeutic effect of urocortin loaded Lf-NP on 6-OHDA rat model of Parkinson's disease. Data are mean ± SEM. $^*p < 0.05$ with respect to the PBS group, $\triangledown p < 0.05$ with respect to the NP-UCN5 group. (A) Apo-induced turns changes of rats in different groups during 3 weeks after the 6-OHDA lesion, $n = 8$. (B) TH-immunoreactivity in the striatum of rats of different groups 3 weeks after the 6-OHDA lesion. (C) Dopamine and its main metabolites DOPAC and HVA percent content in the 6-OHDA lesioned striatum of rats versus the unlesioned side 3 weeks after 6-OHDA lesion, $n = 6$.

again demonstrated that Lf on the surface of nanoparticles could facilitate access of drugs carried by nanoparticles to the brain. In addition, the concentration of coumarin-6 in systemic circulation by Lf-NP was not significantly different from that by NP (Fig. 4C), which suggested the long-circulation characteristic of PEG was not impaired by the conjugation of small amount of Lf.

The pharmacokinetic parameters of coumarin-6 in heart, liver, spleen, lung and kidney after intravenous injection of NP and Lf-NP in mice are shown in Table 3. The AUC of coumarin-6 in different tissues were divided by the corresponding whole blood AUC and the quotients were used to compare the biodistribution behavior of Lf-NP to NP. The calculated AUC_{tissue}/AUC_{blood} results showed that Lf conjugation not only increased the brain delivery but also altered the biodistribution of NP. Compared to the unmodified NP, Lf-NP was more concentrated in heart and spleen, but less distributed to kidney (Fig. 5). The lung and liver distribution of the Lf-NP were not significant different from NP. Although the exact mechanism of this change is unclear, this results remind us of the potential toxicity might be raised by the change of Lf-NP biodistribution.

3.4. Therapeutic effect of UCN-loaded Lf-NP on 6-OHDA rat model of Parkinson's disease

The biodistribution study demonstrated the enhanced delivery of Lf-NP to striatum and substantia nigra regions. The Lf-NP also showed a sustained release behavior, with about 90% incorporated BSA released in PBS (containing 5% plasma) after 15 days (data not shown). To explore the utility of the Lf-NP delivery system in treatment of Parkinson's disease, UCN was incorporated into Lf-NP and injected to the 6-OHDA model rats. The rotation behavior, striatal tyrosine hydroxylase (TH) immunohistochemistry and striatal transmitter contents were used to evaluate the therapeutic effects of UCN-loaded Lf-NP (Lf-NP-UCN). Apomorphine-induced rotation is regarded as a quantitative index of striatal lesion severity (Ungerstedt, 1971). The apomorphine-induced rotations of rats of each group except for the normal group increased with the elapse of time during the 21 days (Fig. 6A). Three weeks later, the rotation behavior of the PBS group was significantly different form that of the normal control group which demonstrated the successful establishment of the 6-OHDA model. The apomorphine-induced turns of Lf-NP-UCN5 group was significantly lower than the PBS and NP-UCN5 groups, while the apomorphine-induced turns of

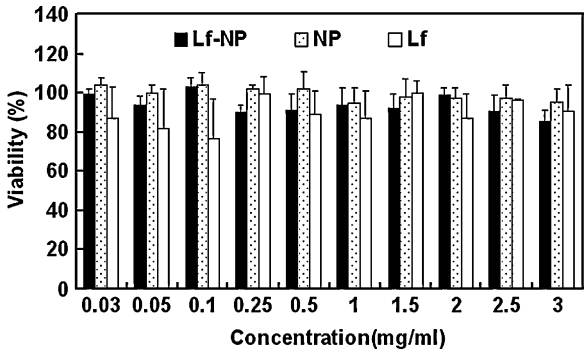

Fig. 7. *In vitro* cytotoxicity of NP, Lf-NP and Lf on bEnd.3 cells at concentrations ranging from 0.025 to 3 mg/ml.

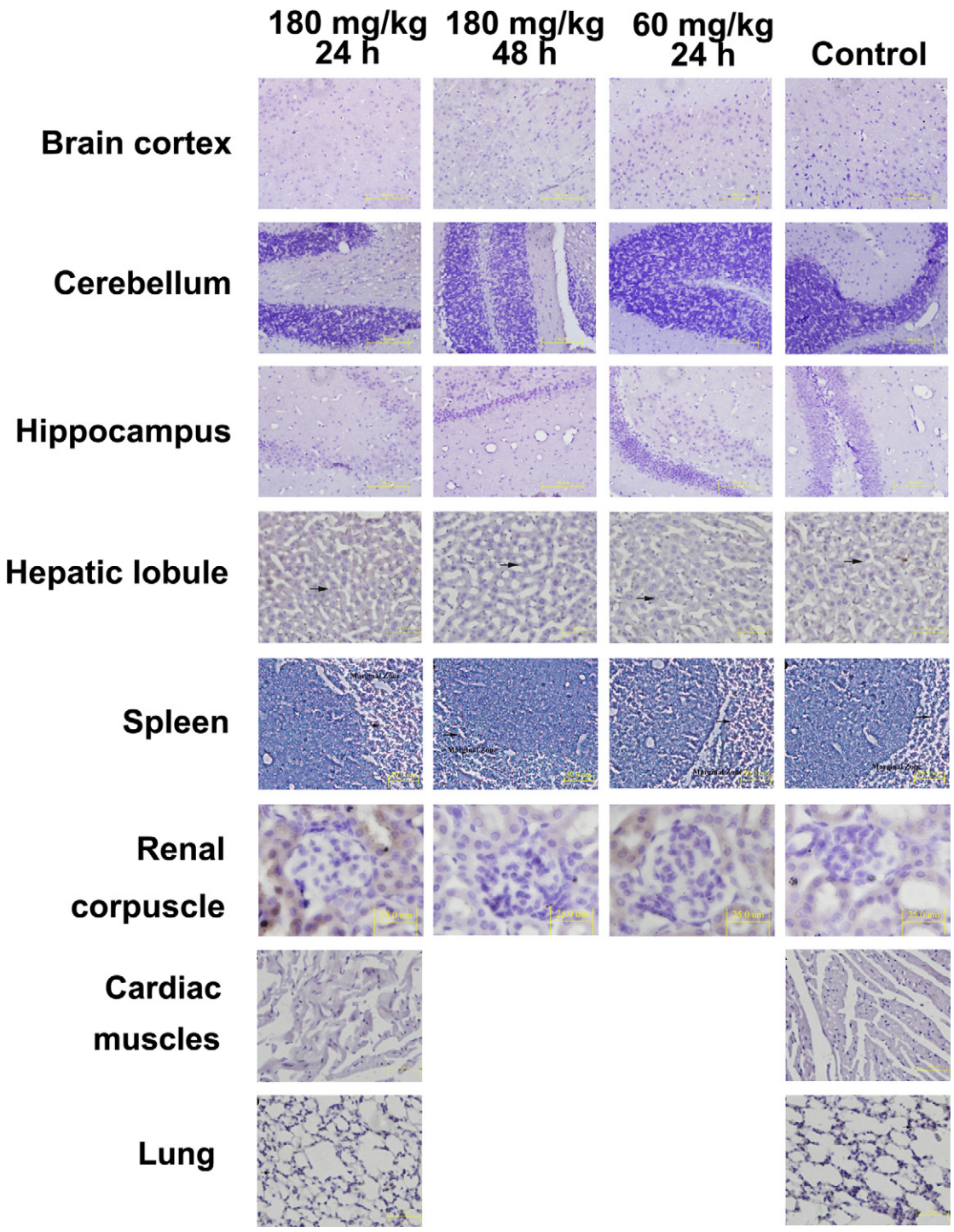

Fig. 8. CD 68 immunohistochemistry of different tissues of BALB/c mice after injected with different doses of Lf-NP one dose per day, for 7 successive days. Cell nuclei were counter-stained with hematoxylin, bar 100 μm.

other experiment groups were not significantly different from the PBS group. The attenuating effect of Lf-NP-UCN5 on the rotation behavior indicated a potential anti-parkinsonian activity. Our findings revealed that tight contralateral rotation was clearly evident in 6-OHDA treated rats three weeks after the surgery but this was greatly attenuated when Lf-NP-UCN5 was injected intravenously the next day after 6-OHDA infusion.

Brain sections from rats after different treatments were analyzed for the TH-immunoreactivity on the 21st day. Normal control group did not show any loss in TH-immunoreactivity in the striatum of the infusion side. Whereas, in the PBS group, striatum region infused with 6-OHDA showed extensive lesion as evidenced by significantly lesser TH-immunoreactive neurons compared to the contralateral side (Fig. 6B). After Lf-NP-UCN5 administration, there was a significant improvement in the TH-immunoreactivity in the 6-OHDA-infused side (Fig. 6B) while the other treatment groups did not show obvious improvement in TH-immunoreactivity.

In order to investigate the change of DA content in the striatum, a validated HPLC-ECD method was used to detect the DA, DOPAC and HVA contents in the striatum, with DOPAC and HVA serving

as indirect indexes of dopamine content. At the 21st day, the percentage contents of the transmitters in the lesioned striatum to the unlesioned side after different treatments were showed in Fig. 6C. The percentage contents of DA, DOPAC and HVA in the PBS group were much lower than that of the normal group, while after Lf-NP-UCN5 treatment, the percentage contents of DA, DOPAC and HVA were significantly higher than that of the PBS group. These results demonstrated that high dose of Lf-NP-UCN had certain effects on increasing DA content in the striatum.

The behavior, immunohistochemistry and transmitter contents results suggested that i.v. injection of 28 μg UCN carried by Lf-NP could effectively attenuate the striatum lesion caused by 6-OHDA. Intracerebral injection of UCN was previously proved to arrest the development of Parkinsonian like features in the rat 6-OHDA paradigms of Parkinson's disease (Abuirmeileh et al., 2007; Kastin et al., 2000). While due to the low BBB permeability of UCN, noninvasive systemic delivery was still impossible. This study for the first time realized the successful noninvasive delivery of UCN to the brain and proved the Lf-NP delivery system was applicable for noninvasive treatment of Parkinson's disease.

3.5. *In vitro and in vivo toxicity of Lf-NP*

Lf conjugation endowed Lf-NP with brain delivery ability, but at the same, changed the biodistribution behavior of the nanoparticles. To investigate the potential toxicity brought by Lf and to further evaluate the safety of the novel delivery system, the toxicity of Lf-NP was studied *in vitro* by cell viability experiment and *in vivo* by CD 68 immunohistochemistry. The *in vitro* cell viability of bEnd.3 cells after incubated for 4 h with different concentrations of Lf, NP and Lf-NP are shown in Fig. 7. The cell viability was always above 85%, even after 4 h incubation with 3 mg/ml Lf-NP, which was not significantly different from the NP and Lf groups. These results demonstrated that the conjugation of Lf did not increase the cytotoxicity of the NP and suggested the Lf-NP delivery system possessed sound biocompatibility.

It is known that the intravenously injected nanoparticles distributed into tissues are uptaken and eliminated by phagocytes (Bazile et al., 1995). CD 68, a specific marker for phagocyte, was used to characterize the acute inflammation of nanoparticles *in vivo* (Lu et al., 2007). An increase in CD 68 expression would indicate increase in inflammatory reactions. The CD 68 immunochemistry results showed that, after successive administration of Lf-NP for 7 days, there were dose-related inflammatory reactions occurred in liver, spleen and kidney at 24 h which further disappeared at 48 h (Fig. 8). Lf-NP showed no obvious inflammatory reactions to other tissues. So i.v. injection of Lf-NP may cause slight or mild transient acute inflammatory reactions in the liver, spleen and kidney. However, further investigations should be concentrated on the long term toxicity and the toxicity on the BBB *in vivo* especially, which could be investigated through morphological evaluation and specific markers expression analysis.

4. Conclusion

A novel Lf-NP brain drug delivery system was constructed by conjugation of biodegradable PEG-PLGA nanoparticles with Lf, a promising brain targeting molecule. The activity of the conjugated Lf was validated by the existence of gold-labeled Lf-NP under TEM and by the ELISA analyses. The significantly increased uptake of the Lf-NP by bEnd.3 cells compared with that of NP could be inhibited by chlorpromazine which demonstrated that Lf-NP was untaken by an additional clathrin related endocytosis process. After a dose of 60 mg/kg Lf-NP or NP injection in mouse caudal vein, the brain coronal section proved a higher accumulation of Lf-NP in the cortex, substantia nigra and striatum region than that of NP. The following pharmacokinetic studies further demonstrated a 2.49 times increase of AUC by Lf-NP than NP in 24 h. UCN-loaded Lf-NP was successfully delivered to the brain and it significantly attenuated the striatum lesion caused by 6-OHDA. Cell viability test and CD 68 immunohistochemistry results proved relatively low toxicity of Lf-NP. The significant *in vitro* and *in vivo* results demonstrated that Lf-NP was a promising brain drug delivery system especially in treating Parkinson's disease. Further work should concentrate on the long term toxicity of Lf-NP.

Acknowledgements

The authors acknowledged Prof. Linyin Feng, Shanghai Institute of Materia Medica, and Head Guiliang Chen, Shanghai Institute for Food and Drug Control, for helping in establishment of rat 6-OHDA Parkinson's model and detection of DA transmitters, respectively. We are also very grateful to Professor Yaocheng Rui, Department of Pharmacology, School of Pharmacy, the Second Military Medical University for providing the immortalized mouse brain endothelial cell line b.End3. This work was supported by National Basic Research Program of China (973 Program) 2007CB935800 and National Science and Technology Major Project 2009ZX09310-006.

References

Abuirmeileh, A., Lever, R., Kingsbury, A.E., Lees, A.J., Locke, I.C., Knight, R.A., Chowdrey, H.S., Biggs, C.S., Whitton, P.S., 2007. The corticotrophin-releasing factor-like peptide urocortin reverses key deficits in two rodent models of Parkinson's disease. Eur. J. Neurosci. 26, 417–423.

Alexis, F., Pridgen, E., Molnar, L.K., Farokhzad, O.C., 2008. Factors affecting the clearance and biodistribution of polymeric nanoparticles. Mol. Pharm. 5, 505–515.

Bazile, D., Prud'homme, C., Bassoullet, M.T., Marlard, M., Spenlehauer, G., Veillard, M., 1995. Stealth Me.PEG-PLA nanoparticles avoid uptake by the mononuclear phagocyte system. J. Pharm. Sci. 84, 493–498.

Beletsi, A., Leontiadis, L., Klepetsanis, P., Ithakissios, D.S., Avgoustakis, K., 1999. Effect of preparative variables on the properties of poly (dl-lactide-co-glycolide)-methoxypoly (ethyleneglycol) copolymers related to their application in controlled drug delivery. Int. J. Pharm. 182, 187–197.

Brown, R.C., Morris, A.P., O'Neil, R.G., 2007. Tight junction protein expression and barrier properties of immortalized mouse brain microvessel endothelial cells. Brain Res. 1130, 17–30.

Calvo, P., Gouritin, B., Chacun, H., Desmaele, D., D'Angelo, J., Noel, J.P., Georgin, D., Fattal, E., Andreux, J.P., Couvreur, P., 2001. Long-circulating PEGylated polycyanoacrylate nanoparticles as new drug carrier for brain delivery. Pharm. Res. 18, 1157–1166.

Choi, J.S., Pham, T.T., Jang, Y.J., Bui, B.C., Lee, B.H., Joo, K.M., Cha, C.I., Lee, K.H., 2006. Corticotropin-releasing factor (CRF) and urocortin promote the survival of cultured cerebellar GABAergic neurons through the type 1 CRF receptor. J. Korean Med. Sci. 21, 518–526.

Davda, J., Labhasetwar, V., 2002. Characterization of nanoparticle uptake by endothelial cells. Int. J. Pharm. 233, 51–59.

De Boer, A.G., Gaillard, P.J., 2007. Drug targeting to the brain. Annu. Rev. Pharmacol. Toxicol. 47, 323–355.

Facci, L., Stevens, D.A., Pangallo, M., Franceschini, D., Skaper, S.D., Strijbos, P.J., 2003. Corticotropin-releasing factor (CRF) and related peptides confer neuroprotection via type 1 CRF receptors. Neuropharmacology 45, 623–636.

Faucheux, B.A., Nillesse, N., Damier, P., Spik, G., Mouatt-Prigent, A., Pierce, A., Leveugle, B., Kubis, N., Hauw, J.J., Agid, Y., 1995. Expression of lactoferrin receptors is increased in the mesencephalon of patients with Parkinson disease. Proc. Natl. Acad. Sci. U.S.A. 92, 9603–9607.

Fillebeen, C., Descamps, L., Dehouck, M.P., Fenart, L., Benaïssa, M., Spik, G., Cecchelli, R., Pierce, A., 1999. Receptor-mediated transcytosis of lactoferrin through the blood–brain barrier. J. Biol. Chem. 274, 7011–7017.

Gabor, F., Schwarzbauer, A., Wirth, M., 2002. Lectin-mediated drug delivery: binding and uptake of BSA-WGA conjugates using the Caco-2 model. Int. J. Pharm. 237, 227–239.

Gosk, S., Vermehren, C., Storm, G., Moos, T., 2004. Targeting anti-transferrin receptor antibody (OX26) and OX26-conjugated liposomes to brain capillary endothelial cells using in situ perfusion. J. Cereb. Blood Flow Metab. 24, 1193–1204.

Grau, A.J., Willig, V., Fogel, W., Werle, E., 2001. Assessment of plasma lactoferrin in Parkinson's disease. Mov. Disord. 16, 131–134.

Hu, K., Li, J., Shen, Y., Lu, W., Gao, X., Zhang, Q., Jiang, X., 2009. Lactoferrin-conjugated PEG-PLA nanoparticles with improved brain delivery: in vitro and in vivo evaluations. J. Control. Release 134, 55–61.

Huang, R.Q., Ke, W.L., Qu, Y.H., Zhu, J.H., Pei, Y.Y., Jiang, C., 2007. Characterization of lactoferrin receptor in brain endothelial capillary cells and mouse brain. J. Biomed. Sci. 14, 121–128.

Huang, R.Q., Ke, W.L., Liu, Y., Wu, D.D., Feng, L.Y., Jiang, C., Pei, Y.Y., 2010. Gene therapy using lactoferrin-modified nanoparticles in a rotenone-induced chronic Parkinson model. J. Neurol. Sci. 290, 123–130.
Huwyler, J., Wu, D., Pardridge, W.M., 1996. Brain drug delivery of small molecules using immunoliposomes. Proc. Natl. Acad. Sci. U.S.A. 93, 14164–14169.
Ji, B., Maeda, J., Higuchi, M., Inoue, K., Akita, H., Harashima, H., Suhara, T., 2006. Pharmacokinetics and brain uptake of lactoferrin in rats. Life Sci. 78, 851–855.
Jones, A.R., Shusta, E.V., 2007. Blood–brain barrier transport of therapeutics via receptor-mediation. Pharm. Res. 24, 1759–1771.
Kastin, A.J., Akerstrom, V., Pan, W., 2000. Activation of urocortin transport into brain by leptin. Peptides 21, 1811–1817.
Kawamata, T., Tooyama, I., Yamada, T., Walker, D.G., McGeer, P.L., 1993. Lactotransferrin immunocytochemistry in Alzheimer and normal human brain. Am. J. Pathol. 142, 1574–1585.
Konstantinos, A., 2004. Pegylated poly (lactide) and poly (lactide-co-glycolide) nanoparticles: preparation, properties and possible applications in drug delivery. Curr. Drug Deliv. 1, 321–333.
Legen, I., Zakelj, S., Kristl, A., 2003. Polarised transport of monocarboxylic acid type drugs across rat jejunum in vitro: the effect of mucolysis and ATP-depletion. Int. J. Pharm. 256, 161–166.
Li, Y., Pei, Y., Zhang, X., Gu, Z., Zhou, Z., Yuan, W., Zhou, J., Zhu, J., Gao, X., 2001. PEGylated PLGA nanoparticles as protein carriers: synthesis, preparation and biodistribution in rats. J. Control. Release 71, 203–211.
Liu, J., Shapiro, J.I., 2003. Endocytosis and signal transduction: basic science update. Biol. Res. Nurs. 5, 117–128.
Lu, W., Zhang, Y., Tan, Y.Z., Hu, K.L., Jiang, X.G., Fu, S.K., 2005. Cationic albumin-conjugated pegylated nanoparticles as novel drug carrier for brain delivery. J. Control. Release 107, 428–448.
Lu, W., Wan, J., She, Z., Jiang, X., 2007. Brain delivery property and accelerated blood clearance of cationic albumin conjugated pegylated nanoparticle. J. Control. Release 118, 38–53.
Mehdipour, A.R., Hamidi, M., 2009. Brain drug targeting: a computational approach for overcoming blood–brain barrier. Drug Discov. Today 14, 1030–1036.
Mo, Y., Lim, L.Y., 2004. Mechanistic study of the uptake of wheat germ agglutinin-conjugated PLGA nanoparticles by A549 cells. J. Pharm. Sci. 93, 20–28.
Moos, T., Morgan, E.H., 2001. Restricted transport of anti-transferrin receptor antibody (OX26) through the blood–brain barrier in the rat. J. Neurochem. 79, 119–129.
Olivier, J.C., Huertas, R., Lee, H.J., Calon, F., Pardridge, W.M., 2002. Synthesis of pegylated immunonanoparticles. Pharm. Res. 19, 1137–1143.
Panyam, J., Sahoo, S.K., Prabha, S., Bargar, T., Labhasetwar, V., 2003. Fluorescence and electron microscopy probes for cellular and tissue uptake of poly(D,L-lactide-coglycolide) nanoparticles. Int. J. Pharm. 262, 1–11.
Pardridge, W.M., 2007. Blood–brain barrier delivery. Drug Discov. Today 12, 54–61.
Paxinos, G., Watson, C., 1998. The Rat Brain in Stereotaxic Coordinates. Academic Press, San Diego.
Pederson, W.A., Wan, R., Zhang, P., Mattson, M.P., 2002. Urocortin, but not urocortin II, protects cultured hippocampal neurons from oxidative and excitotoxic cell death via corticotropin-releasing hormone receptor type 1. J. Neurosci. 22, 404–412.
Seto, E.S., Bellen, H.J., Lloyd, T.E., 2002. When cell biology meets development: endocytic regulation of signaling pathways. Genes Dev. 16, 1314–1316.
Sharma, A., Sharma, S.U., 1997. Liposomes in drug delivery: progress and limitations. Int. J. Pharm. 154, 123–140.
Spik, G., Legrand, D., Leveugle, B., Mazurier, J., Mikogami, T., Montreuil, J., Pierce, A., Rochard, E., 1994. Characterisation of two kinds of lactotransferrin (lactoferrin) receptors on different target cells. Adv. Exp. Med. Biol. 357, 13–19.
Suzuki, Y.A., Lopez, V., Lönnerdal, B., 2005. Mammalian lactoferrin receptors: structure and function. Cell Mol. Life Sci. 62, 2560–2575.
Ungerstedt, U., 1971. Adipsia and aphagia after 6-hydroxydopamine induced degeneration of the nigro-striatal dopamine system. Acta Physiol. Scand. Suppl. 367, 95–122.
Zhang, Y., Zhu, C., Pardridge, W.M., 2002. Antisense gene therapy of brain cancer with an artificial virus gene delivery system. Mol. Ther. 6, 67–72.
Zhang, Y., Calon, F., Zhu, C., Boado, R.J., Pardridge, W.M., 2003. Intravenous nonviral gene therapy causes normalization of striatal tyrosine hydroxylase and reversal of motor impairment in experimental parkinsonism. Hum. Gene Ther. 14, 1–12.